

# Evaluation of minimum-to-severe global and macrovesicular steatosis in human liver specimens: a portable ambient light-compatible spectroscopic probe

Hao Guo<sup>1</sup>, Ashley E. Stueck<sup>2</sup>, Jason B. Doppenberg<sup>3</sup>, Yun Suk Chae<sup>3</sup>, Alexey B. Tikhomirov<sup>1</sup>, Haishan Zeng<sup>4</sup>, Marten A. Engelse<sup>3</sup>, Boris L. Gala-Lopez<sup>5</sup>, Anita Mahadevan-Jansen<sup>6</sup>, Ian P.J. Alwayn<sup>3</sup>, Andrea Locke<sup>6</sup>, and Kevin Hewitt<sup>1</sup>

<sup>1</sup>Dalhousie University Department of Physics and Atmospheric Science

<sup>2</sup>Dalhousie University Department of Pathology

<sup>3</sup>Leids Universitair Medisch Centrum

<sup>4</sup>British Columbia Cancer Agency

<sup>5</sup>Dalhousie University Department of Surgery

<sup>6</sup>Vanderbilt University

July 16, 2024

## Abstract

This study presents a portable spectroscopic system compatible with ambient light to assess hepatic steatosis (HS) and macrovesicular steatosis (MaS) in human liver specimens. Traditional assessment methods for MaS are limited, prompting the need for non-invasive alternatives. The study utilized a two-stage approach on thawed snap-frozen liver specimens. Biochemical validation compared fat content from Raman and reflectance intensities with triglyceride (TG) quantifications, while histopathological validation contrasted Raman-derived fat content with pathologist evaluations and an algorithm. Analysis of 16 specimens showed a positive correlation between spectroscopic data and TG quantifications. The Raman system differentiated various degrees of global HS and MaS in an additional 66 specimens. A dual-variable prediction algorithm classified significant discrepancies ([?]10%) between algorithm-estimated global HS and pathologist-estimated MaS. This study demonstrates the viability of a portable spectroscopic system for non-invasive HS and MaS assessment to enhance real-time donor liver assessments during recovery to improve transplantation outcomes.

## Evaluation of minimum-to-severe global and macrovesicular steatosis in human liver specimens: a portable ambient light-compatible spectroscopic probe

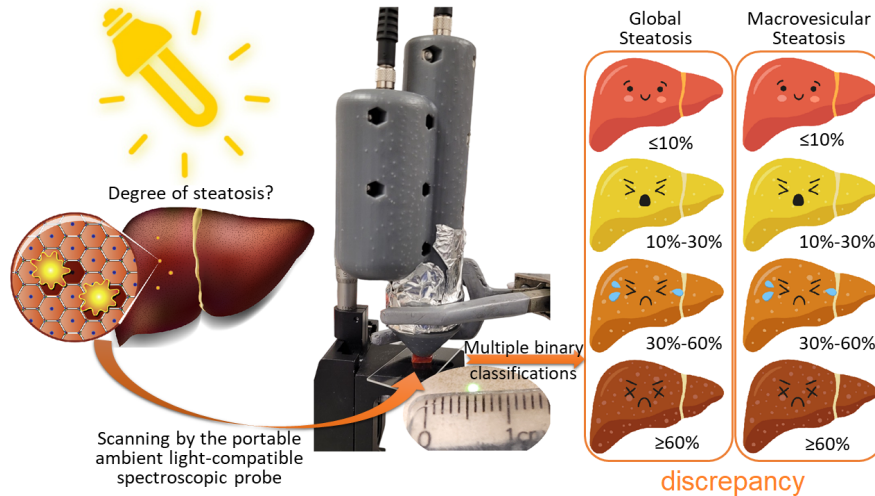
### Financial support

This study was supported by the Early-Stage Commercialization Fund Phase-II, Innovacorp, Innovation Mobilization Program, and Springboard Atlantic.

H.G. was supported by the Vitamin Scholarship, Dalhousie University and the Research Nova Scotia Doctoral Award, Research Nova Scotia.

### Acknowledgement

The authors thank Menno Hoekstra for training H.G. and Y.S.C. for triglyceride quantification of liver tissues. The authors also thank Lab2Market, Ready2Launch, and ideaHUB for vital technical and financial support in developing and iterating our prototype systems.



## Highlights

- We introduced a portable ambient light-compatible spectroscopic probe which could non-invasively analyze Raman scattering and reflectance of human liver specimens.
- Both biochemical and histopathological approaches were applied to validate the spectroscopic probe.
- Histopathological evaluation covered minimum-to-severe global and macrovesicular steatosis, surpassing previous spectroscopic studies.
- A dual-variable prediction for precise differentiation between global and macrovesicular steatosis offers the potential for enhanced, real-time, and quantitative liver assessments in clinical settings.

## Evaluation of minimum-to-severe global and macrovesicular steatosis in human liver specimens: a portable ambient light-compatible spectroscopic probe

Hao Guo, Ashley E. Stuec, Jason B. Doppenberg, Yun Suk Chae, Alexey B. Tikhomirov, Haishan Zeng, Marten A. Engelse, Boris L. Gala-Lopez, Anita Mahadevan-Jansen, Ian P.J. Alwayn, Andrea K. Locke, and Kevin C. Hewitt

**Abstract:** This study presents a portable spectroscopic system compatible with ambient light to assess hepatic steatosis (HS) and macrovesicular steatosis (MaS) in human liver specimens. Traditional assessment methods for MaS are limited, prompting the need for non-invasive alternatives. The study utilized a two-stage approach on thawed snap-frozen liver specimens. Biochemical validation compared fat content from Raman and reflectance intensities with triglyceride (TG) quantifications, while histopathological validation contrasted Raman-derived fat content with pathologist evaluations and an algorithm. Analysis of 16 specimens showed a positive correlation between spectroscopic data and TG quantifications. The Raman system differentiated various degrees of global HS and MaS in an additional 66 specimens. A dual-variable prediction algorithm classified significant discrepancies ( $\geq 10\%$ ) between algorithm-estimated global HS and pathologist-estimated MaS. This study demonstrates the viability of a portable spectroscopic system for non-invasive HS and MaS assessment to enhance real-time donor liver assessments during recovery to improve transplantation outcomes.

**Abbreviations used in this paper :** AUROC, area under the operating characteristic curve; HS, hepatic steatosis; LT, liver transplantation; LUMC, Leiden University Medical Center; MaS, macrovesicular steatosis; MiS, microvesicular steatosis; OR, operating room; ORO, Oil Red O; ROC, receiver operating characteristic; SD, standard deviation; TG, triglyceride; VUMC, Vanderbilt University Medical Center

# Introduction

Hepatic steatosis (HS), particularly macrovesicular steatosis (MaS) in donor livers, has been found to be linked to a higher likelihood of graft dysfunction following liver transplantation (LT).<sup>1,2</sup> Severe MaS (>60%) is typically viewed as high risk and leads to organs being discarded.<sup>3</sup> As the donor liver pool expands to accommodate the growing number of patients on waiting lists, it is increasingly essential to conduct thorough assessments of survival benefits among candidates.<sup>4,5</sup> High-quality estimations of risk factors are crucial, as donors with less favourable characteristics are now more frequently considered for transplantation. The recovery rate of donor livers with moderate (30%-60%) MaS has increased over the years, while other risk factors of mortality or graft loss were mitigated<sup>6,7</sup>. However, the discard rate of moderately and severely steatotic livers is still high because of their higher risk of graft dysfunction.<sup>8,9</sup> According to a recent study on 17,801 liver transplant recipients, compared with recipients of grafts with 0-10% MaS, the hazard of graft failure was found to be 53% and 25% higher among the recipients of grafts with >30% MaS and 10%-30% MaS, respectively.<sup>10</sup> Therefore, precise classifications and quantification of steatotic donor livers, alongside a clear-cut threshold at different degrees of MaS, are crucial for optimizing liver allocation and maximizing the survival benefit of liver recipients. At present, donor livers are assessed macroscopically at the time of recovery.<sup>11</sup> This assessment is often subjective and dependent on the experience of the donor surgeon. If necessary, frozen sections can be obtained, but this often is associated with significant delays and requires the availability of an expert pathologist.<sup>12</sup> A tool that can provide objective, quantitative and rapid analysis of (donor) liver fat content is needed. Optical spectroscopic tools, including infrared (IR), reflectance, and Raman, have shown significant potential in evaluating HS due to their minimally invasive nature and rapid analysis capabilities.<sup>11,13</sup> Recent studies on both animal models and human livers have demonstrated that IR spectroscopy<sup>14-16</sup> and reflectance spectroscopy<sup>17,18</sup> could evaluate various degrees of global HS (with out differentiating MaS); however, those applications required either switching off (directing away) surgical lights or using an invasive optical needle in the operating room (OR). Furthermore, complex spectral analyses of acquired data were a necessity. Raman spectroscopy offers some distinct advantages. It is sensitive to rotations and vibrations of chemical bonds, making its inherent high molecular specificity ideal for characterizing biological materials.<sup>11,19</sup> Pre-clinical studies on *ex vivo* rodent liver specimens revealed that Raman spectroscopy could quantify HS in animal models using signals in the high wavenumber region 2800–3000  $\text{cm}^{-1}$ , and the results agreed well with pathology ratings.<sup>20-22</sup> Confocal Raman microscopy has been reported to effectively analyze the sizes of lipid droplets in rodent livers.<sup>23-25</sup> This offers insights relevant to microvesicular steatosis (MiS) and MaS. However, obtaining a Raman image can be considered too time-consuming to be helpful when assessing the HS of donor livers, as each pixel requires spectral analyses. The exploration of HS in LT using conventional Raman spectroscopy lags IR and reflectance spectroscopy. Hewitt et al. (2015)<sup>20</sup> and Pacia et al. (2018)<sup>21</sup> proved the concept that conventional Raman spectrometers could assess the fat content of rodent livers. However, neither of the two studies discussed HS assessment at morphological levels. Navigating the challenges associated with weak signal detection and fluorescence interferences, we engineered a filter-based 1064-nm Raman system validated through examinations using phantom models and duck liver samples.<sup>26</sup> In our previous study, employing readily interpretable voltage intensities to quickly quantify the relative fat content within the examined liver samples, this multi-channel system functioned reliably ( $r^2 = 0.934$ ) under normal and intense ambient light conditions<sup>26</sup>. In the present study, we analyzed 95 specimens in two sets from two medical centers, utilizing our filter-based 1064-nm Raman system. For the initial set of 16 specimens, fat contents converted from Raman and reflectance intensities were contrasted with triglyceride (TG) quantification results. Subsequently, for the more extensive set of 66 specimens, fat contents derived from Raman and reflectance intensities were compared to evaluations of MaS and global HS (including MiS and MaS) performed by an expert pathologist and to determinations of positive pixels made by an algorithm.

# Materials and Methods

not-yet-known not-yet-known

not-yet-known

unknown

1 Design of the study The study employed a two-stage approach to ascertain the validity of Raman spectroscopy technique in assessing the degree of steatosis in human liver specimens, as demonstrated in Figure 1 .

1 Design of the study

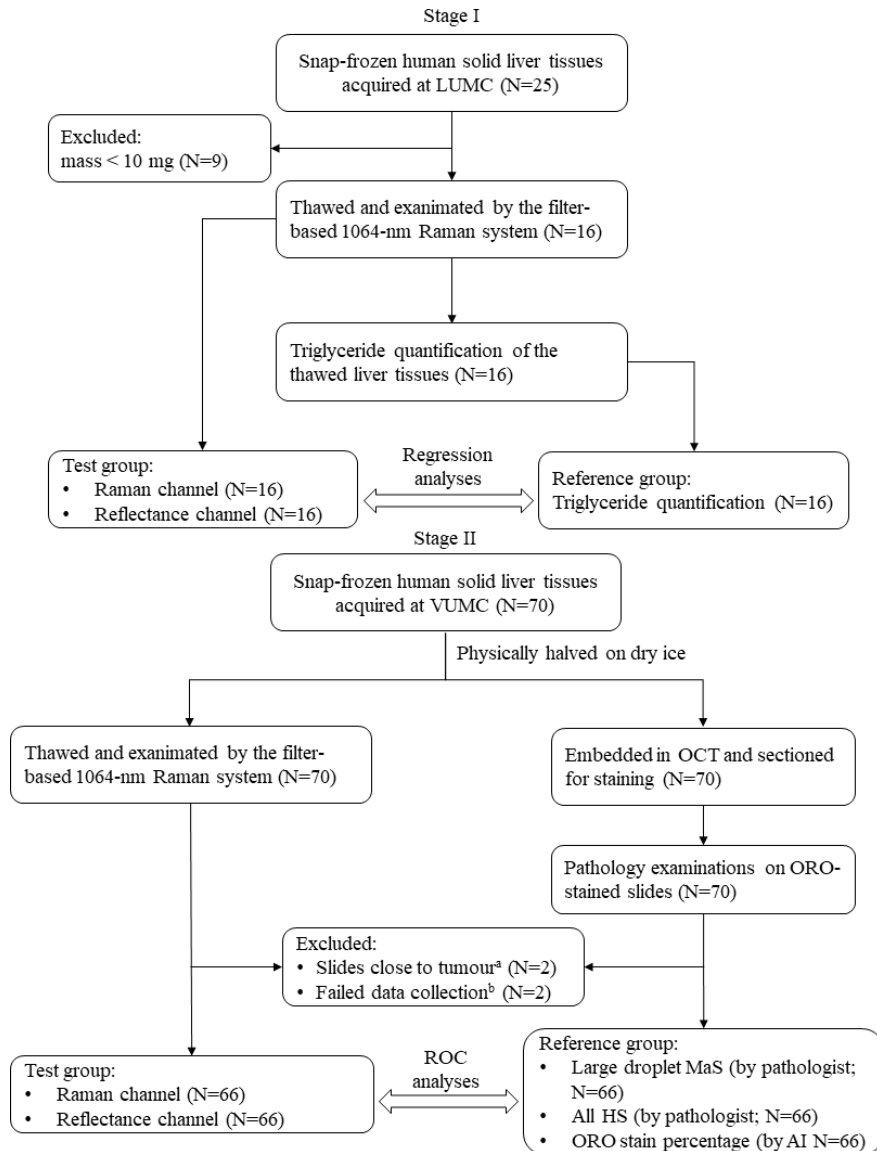


Figure 1. Flow chart of the present study. (a) The specimens had tumours, and the stained frozen section was physically close to the tumour. (b) The SD of voltage signals in either channel was greater than 80  $\mu$ V.

## Stage I: biochemical validation

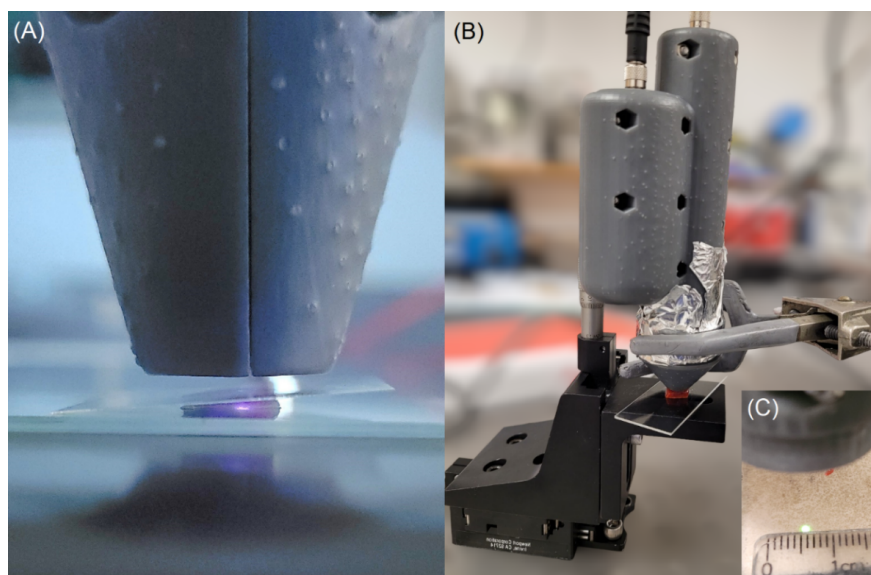
In the first stage, we studied 25 snap-frozen human liver specimens (weighing between 1.3 mg and 58.1 mg): 24 from remnants of pre- and post-LT wedge biopsies and one from a discarded donor liver at Leiden University Medical Center (LUMC) in August 2022. The specimens were thawed at room temperature and scanned using the Raman system under ambient room light. The liver specimens were refrozen at -80 degrees Celsius and thawed again for TG quantification. Given that the penetration depth of the incident laser beam was at least 1mm,<sup>26</sup> only specimens heavier than 10 mg (thicker than 1 mm) were included to avoid the insufficiency to quantify TG of low-mass specimens<sup>27,28</sup>. The fat content derived from the analyses using the Raman and reflectance channels was then compared with the TG quantification results to assess the Raman system's accuracy in steatosis estimation.

## Stage II: histopathological validation

In the second stage, at Vanderbilt University Medical Center (VUMC) in November 2022, 70 snap-frozen human liver specimens weighing between 0.24 g and 2.58 g were obtained through the Cooperative Human Tissue Network. These liver specimens were split on dry ice: one half was thawed in cold water and scanned under ambient light using the investigated Raman system, while the other half was cryo-sliced and stained with Oil Red O (ORO) for histological analysis. The Raman system user (HG) and the expert pathologist (AES) performed the Raman and histopathological assessments independently, blinded to the results of each other assessment. Four liver specimens were excluded due to proximity to tumours or due to Raman data collection issues. The Raman results were compared to expert pathologist evaluations of steatosis.

## Spectroscopical evaluation of fat content

In the biochemical validation stage: Stage I (Figure 2A), data collection lasted 10 seconds at 28 recordings per second. Data collection in the histopathological validation stage: Stage II (Figure 2B) lasted 20 seconds at ten recordings per second.



## Statistical methods

Stata version 18.0-Basic Edition (StataCorp LLC, TX, USA) was used for statistical analyses. Logistic regression was performed, and performance of the investigated Raman system in HS prediction was evaluated through serial binary classifications and corresponding Receiver Operating Characteristic (ROC) analyses. As a non-parametric test, the Mann-Whitney U test was used to compare whether there is a significant difference in the distributions of two groups of samples after classification.

## Results

This study included 16 and 66 human liver specimens in the biochemical and histopathological validation stages for analyses. The characteristics of the population are shown in **Table 1**. The ethnicity information was not available in the biochemical validation stage, as it is not routinely captured in the LUMC database. **Figure 3** shows that the fat contents obtained from the Raman system measurements are positively correlated with triglyceride levels. These correlations imply that signals of both the reflectance and Raman channels contained information about fat contents in human specimens. It should be noted that the reflectance channel signals had a worse linear correlation coefficient than the Raman channel (0.64 vs. 0.82). Typical liver specimens with minimum triglyceride contents between 0.2  $\mu\text{g}/\mu\text{g}$  protein and 0.4  $\mu\text{g}/\mu\text{g}$  protein were predicted to have more than 40% fat in content, implying that the calibration using duck fat-agar phantoms resulted in a significant zero-point error of the reflectance channel.

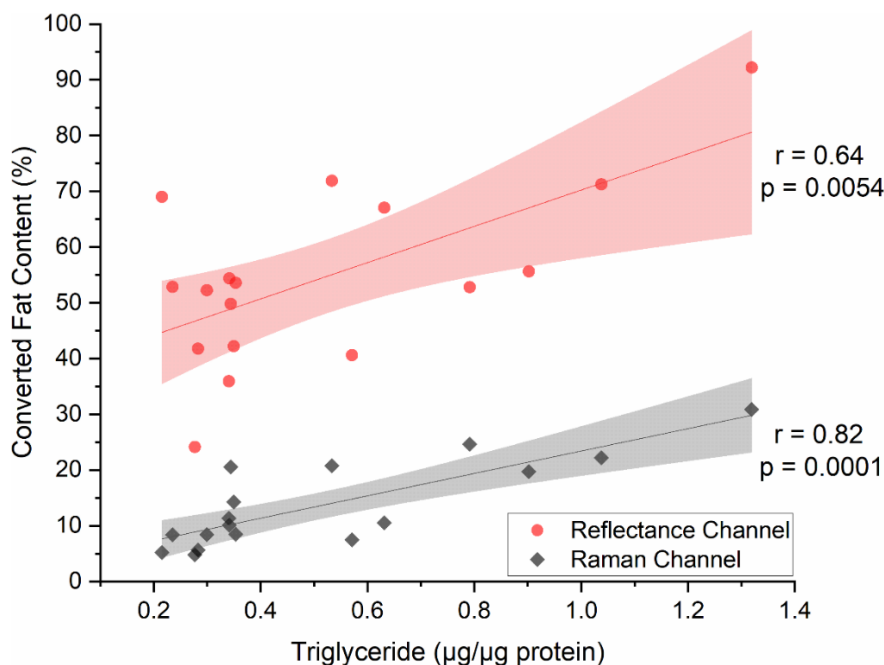


Figure 3. Plots and linear regressions of triglyceride content vs. converted fat contents from voltage signals of the reflectance and Raman channels. Shadow areas: 95% confidence bands of linear regressions.

An expert liver pathologist (AES) assessed the whole slide images (as shown in **Figure 4A**) and estimated, to the nearest 5% interval, the percent of large droplet MaS and the percent of global (macro- and micro-vesicular) HS. The assessment of large droplet MaS was performed per the most recent Banff recommendations<sup>12</sup> for “large droplet fat,” defined as a single droplet expanding the hepatocyte and larger than adjacent cells, with low power determination of the percentage of tissue affected, followed by higher

magnification assessment of fatty areas to determine what proportion of steatotic cells meet the definition of “large droplet fat,” and finally adjustment of the low power percentage accordingly. After completion of pathologist estimates, positive pixels (as shown in **Figure 4B**) were counted automatically using the Positive Pixel Count algorithm v9 of Aperio ImageScope (Leica Biosystems); this value was normalized by the area assessed to generate a percentage. Areas of artifact, such as tissue folding or coverslip lifting, were manually excluded from the analysis.

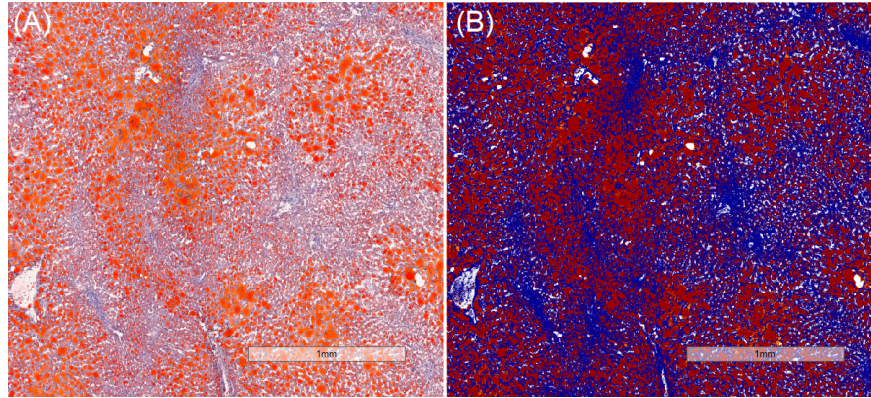


Figure 4. (A) Original view and (B) view after applying the Positive Pixel Count algorithm v9 of digitized images of an ORO-stained frozen section at 40X magnification. The expert pathologist (AES) assessed global HS and MaS based on the original view, and the algorithm quantified the ORO stain percentage based on the stained slide pixel area. The ORO-stained lipid droplets (positive pixels) are in orange (A) in brightfield and in red (B) after the application of the Positive Pixel Count algorithm v9.

Considering the better linear correlation of the Raman signal with the TG results in the biochemical validation stage, compared to the Reflectance measurements, the Raman signal was used as the primary variable for predicting HS in the histopathological validation stage. The boxplots in **Figure 5** show the distribution of fat content estimated by the Raman system, grouped by the degree of large droplet MaS (assessed by the expert pathologist), ORO stain percentage (estimated by the algorithm), and total steatosis percentage (evaluated by the expert pathologist).

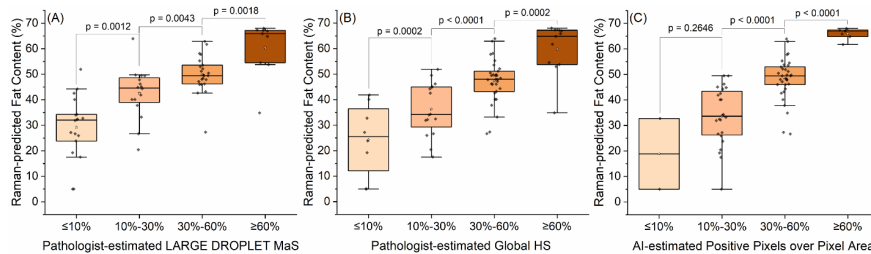


Figure 5. Boxplots of Raman-estimated fat content vs. (A) grade of pathologist-estimated large droplet macrosteatosis, (B) pathologist-estimated all steatosis in percentage (to the nearest 5%), and (C) the algorithm-estimated Oil Red O-stained pixels over pixel area (of Oil Red O-stained slides) in percentage. The boxes represent the interquartile range, with the horizontal lines inside the box indicating the median fat content values. The blank stars inside the box represent the mean fat content values. The whiskers extend from the boxes to represent the minimum and maximum fat content values, excluding any outliers (the 1.5xIQR rule applied) plotted as individual dots outside the whiskers.

Logistic regression (using the “**logit**” command) revealed significant (all p-values < 0.0001) differences in

the Raman-estimated fat content among all groups. As shown in **Table 2**, the Raman-estimated fat content, as a single predictor (using the “**predict**” command), effectively differentiated minimum risk ([?]10%), low-risk (10%-30%), high-risk (30%-60%), and maximum-risk ([?]60%) MaS and global HS, with areas of the operating characteristic curve (AUROC) between 0.88 and 0.90.

Utilizing both Raman and reflectance signals enhanced the AUROC of almost all binary classifications; however, the differences between the Raman and dual-channel predictions were insignificant (see **Table S1**).

Most specimens in the pathological validation stage had a mixed form of MaS and MiS. As **Figure 6(A-B)** shows, the degree of MaS of the studied liver specimens was strongly positively correlated with the degrees of pathologist-estimated global HS and the algorithm-estimated positive pixel area, limiting examinations of the investigated Raman system on distinguishing MaS from global HS.

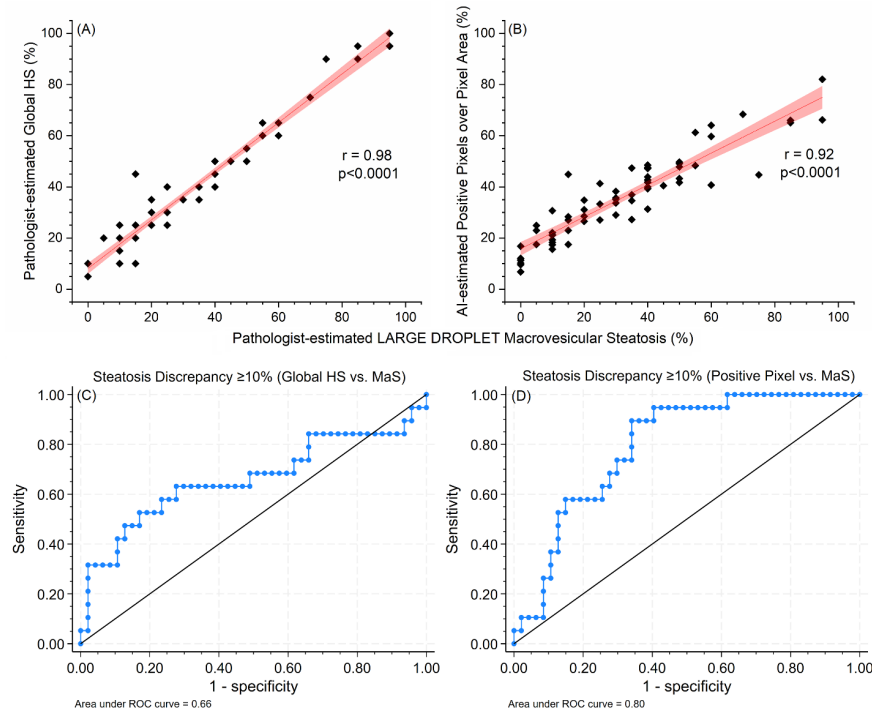


Figure 6. (A-B) Plots and linear regressions of (A) pathologist-estimated global HS vs. pathologist-estimated MaS and (B) the algorithm-estimated global HS vs. pathologist-estimated MaS. (C-D) ROCs of dual-variable binary predictions on [?]10% steatosis discrepancy between (C) pathologist-estimated global HS and pathologist-estimated MaS and (D) algorithm-estimated global HS and pathologist-estimated MaS. The Raman and the reflectance channels were applied as dual predictors.

Considering the inherently high correlation with global HS (assessed by the expert pathologist and the algorithm) and the pathological assessments are to the nearest 5% steatosis, we set a compromised steatosis discrepancy threshold at 10%. Information from the reflectance channel was paired with the Raman-estimated fat content for dual-variable predictions. **Figure 6(C)** shows the ROC curves of binary predictions on [?]10% steatosis discrepancy between pathologist-estimated global HS and pathologist-estimated MaS, with an AUROC of 0.66. This could be due to data points’ degradation (overlapping), as the expert pathologist’s estimations were to the nearest 5%.

The ROC curve of binary predictions on [?]10% steatosis discrepancy between the algorithm-estimated global HS (positive pixel area) and pathologist-estimated MaS presented a better AUROC of 0.80, as shown

in **Figure 6(D)** . This may be attributed to the algorithm-based estimation of global HS, which quantified the areas of ORO-stained lipid droplets in liver specimens, yielding more precise percentage readings.

## Discussion

The accumulation of TGs within hepatocytes is characteristic of HS.<sup>35</sup> Raman spectroscopy has been validated to assess liver steatosis in animal models based on characteristic Raman peaks.<sup>20,21</sup> While the calibration of the investigated Raman system was in keeping with previous reports,<sup>26</sup> the investigated Raman system demonstrated substantial positive correlations with both Raman ( $r = 0.82$ ) and reflectance ( $r = 0.64$ ) channels, indicating its capability to assess TG in liver specimens. This made it suitable for further evaluation in the histopathological validation stage. In the histopathological validation stage, the Raman channel was revealed to be able to classify MaS and global HS of human liver specimens. Combining information from the two channels, dual-variable predictions of 66 liver specimens reported good (AUROC = 0.80) classification of an [?]10% steatosis discrepancy between pathologist-estimated MaS and the algorithm-estimated HS (ORO-stained pixel area). These findings indicated that the investigated ambient light-compatible Raman system was capable of accurate ex-situ evaluation of global HS in human livers. The investigated Raman system has demonstrated preliminary efficacy in MaS assessments, indicating its potential as a valuable tool for the in-situ real-time surgical evaluation of donor liver steatosis. The primary strength of the present study lies in the multifaceted correlation of Raman assessments with a robust array of subjective and objective references. This included TG quantification, expert pathologist evaluation, and advanced the algorithm-based estimation, achieving validations from diverse and complementary perspectives. Moreover, the observed steatosis within the specimens in the histopathological validation stage exhibited a broad distribution of minimum-to-severe steatosis, facilitating a comprehensive evaluation of the HS classifications through the investigated Raman system. This wide-ranging analysis underscores the potential of our approach in advancing the understanding of integrated spectroscopic evaluation on HS and may pave the way for surgical diagnostic techniques. All specimens included in this study were initially snap-frozen. Although the specimens could not represent donor livers for recovery, their chemical compositions (to which Raman spectroscopy is sensitive) and morphology were to a great extent comparable to those of donor liver organs. All the specimens studied in the pathological validation stage were several times thicker than the 1-mm laser penetration depth reported in the previous clinical trial,<sup>26</sup> enabling enough scattering interaction as a shone liver organ would provide. This study encountered several limitations in evaluating the Raman system for HS assessment. A significant hurdle was the mixed presence of MaS and MiS in most specimens, complicating the distinction between MaS and global HS. During the biochemical validation stage, the exclusion of 9 out of 25 specimens due to their size and weight markedly diminished the statistical power, and the reliance on duck fat-agar phantoms for setting up a “zero point” by calibration hampered the system’s accuracy and convenience. The research noted a promising dual-variable prediction based on Raman scattering and reflectance, capable of classifying specimens with a minimum 10% greater global HS than MaS. However, this finding, lacking a solid physicochemical basis, necessitates further exploration. van Staveren et al. (1991) accurately predicted the scattering coefficient of fat emulsion Intralipid-10% using Mie theory and the size distribution of lipid particles.<sup>36</sup> A reasonable guess is that the reflectance channel (Mie scattering) contained information about both fat content and lipid droplet size; however, more studies according to the physical principles of Raman and Mie scattering, e.g., Monte Carlo simulations, are needed to probe the concept of the dual-variable prediction. Additionally, the untested performance of the Raman system in operating room conditions, despite its proven resistance to 10,000 lm LED light in laboratory settings, leaves a significant gap in understanding its comprehensive compatibility.<sup>26</sup> In this study, a single expert pathologist (AES) assessed all microscopic slide images and estimated the percentage of large droplet MaS and global HS. Despite the potential for diverse insights from multiple pathologists,<sup>37,38</sup> we opted for a single expert to ensure consistent assessment methods and mitigate the risk of interobserver discordance. This approach also assured the quality of the assessment, leveraging the pathologist’s high expertise. The Positive Pixel Count algorithm, as an additional independent approach to quantify the fat content, validated the pathologist’s estimations

and enabled finer quantitative discrepancy of global HS and MaS. To the best of the authors’ knowledge, the present study represents the inaugural trial of conventional Raman spectroscopy on human liver specimens for HS assessment. Advancing beyond the scope of preceding Raman studies, this research emphasized an ambient light-compatible methodology. The efficacy of the Raman spectroscopic approach in assessing the HS of human liver specimens was validated by correlating the fat content results provided by the examined Raman system with TG quantifications. Additionally, histopathological validation was conducted across a wide range of steatotic human liver specimens, culminating in the development of a dual-variable prediction for significant discrepancies (>10%) between global HS and MaS. The insights gained from this study may contribute to enhancing other spectroscopic surgical instruments.

## Conclusion

This research marks a novel endeavour in utilizing a portable spectroscopic system to assess hepatic steatosis in human liver specimens. Two-stage biochemical and histopathological validations highlight the potential of the examined system as a trustworthy, non-invasive modality for steatosis evaluation. Notably, the ambient light-compatible approach signifies a notable progression beyond prior spectroscopic methods, effectively addressing associated limitations. Raman scattering was validated able to quantify lipid content and therefore detect the presence of Global HS in human liver specimens. Moreover, introducing a dual-variable prediction for identifying significant ([?]10%) discrepancies in global HS and MaS demonstrates the potential of differentiating between steatotic livers with different extent of MaS. Beyond immediate outcomes, this study lays the foundation for the broader application of ambient light-compatible spectroscopic probes in clinical environments, potentially revolutionizing intraoperative liver assessments. Amidst the escalating demand for liver transplantation, tools of this nature hold substantial promise in ensuring optimal graft quality, consequently benefiting liver recipients. While the results are encouraging, further research is imperative to affirm the comprehensive potential and applicability of this system, especially in real-world operating room contexts. Table 1. Population characteristics of included human liver specimens.

	Stage I: Biochemical Validation	Stage II: Histopathological Validation
Included Liver Specimen Size, n	16	66
Age, year, mean ± SD	*42.9 ± 13.6	55.7 ± 13.1
Male, %	60.0	45.4
Female, %	40.0	54.6
Specimen Weight, mg, mean ± SD	22.1 ± 12.2	1052.1 ± 589.9
Race/Ethnicity		
Asian, n (%)	N/A	2 (3.0)
Black, n (%)	N/A	5 (7.6)
Hispanic, n (%)	N/A	1 (1.5)
Indigenous, n (%)	N/A	1 (1.5)
White, n (%)	N/A	57 (86.4)
Data from 15 specimens were available.		

Table 2. AUROCs of the binary predictions of the Raman channel in differentiating between specimens of MaS, (pathologist-estimated) global HS, and (algorithm-estimated) ORO stain percentage based on stained slide pixel area at different thresholds. CI: confidence interval.

Threshold	MaS	95% CI	Global HS	95% CI	Positive Pixel Area	95% CI
10%	0.90	[0.82-0.99]	0.90	[0.80-0.99]	0.89	[0.70-1.00]
30%	0.88	[0.80-0.96]	0.88	[0.80-0.96]	0.88	[0.80-0.96]

Threshold	MaS	95% CI	Global HS	95% CI	Positive Pixel Area	95% CI
60%	0.90	[0.75-1.00]	0.90	[0.75-1.00]	0.90	[0.75-1.00]

## Ethics Statement

Ethical review and approval were not required for the study at Leiden University Medical Center on human liver specimens by the local legislation and institutional requirements. The Institutional Review Board at Vanderbilt University approved the study at Vanderbilt University (IRB #: 121423). Both studies were approved by the Health Sciences Research Ethics Board at Dalhousie University (REB #: 2022-6133 and 2022-6318).

## Declaration of AI and AI-assisted technologies in the writing process

Statement: During the preparation of this work, the authors used ChatGPT-4 (Open AI, San Francisco, CA, USA) in order to improve readability and language. After using this tool, the authors reviewed and edited the content as needed and take full responsibility for the content of the publication.

## Author’s contributions

H.G., A.B.T., H.Z., B.L.G-L., I.P.J.A., and K.C.H. contributed to the conception. All authors contributed to the design of the study. H.G., A.E.S., J.B.D, Y.S.C., and A.K.L. contributed to the data acquisition in the study. H.G., A.E.S., Y.S.C., and K.C.H. analyzed the data. H.G. and A.E.S. drafted the manuscript. H.Z., M.A.E., B.L.G-L., A.M-J., I.P.J.A., A.K.L., and K.C.H. oversaw the research project and provided guidance. All the authors critically reviewed the manuscript and provided final approval of the manuscript for publication.

## Reference

1. Moosburner S, Gassner JMGV, Nösser M, Pohl J, Wyrwal D, Claussen F, Ritschl P V., Dragun D, Pratschke J, Sauer IM, Raschzok N. Prevalence of steatosis hepatitis in the eurotransplant region: Impact on graft acceptance rates. *HPB Surg*, 2018, 20182. Orman ES, Barritt AS, Wheeler SB, Hayashi PH. Declining liver utilization for transplantation in the United States and the impact of donation after cardiac death. *Liver Transplant*, 2013, 19:59–683. Linares I, Hamar M, Selzner N, Selzner M. Steatosis in Liver Transplantation: Current Limitations and Future Strategies. *Transplantation*, 2019, 103:78–904. deLemos AS, Vagefi PA. Expanding the donor pool in liver transplantation: Extended criteria donors. *Clin Liver Dis*, 2013, 25. Volk ML, Roney M, Merion RM. Systematic bias in surgeons’ predictions of the donor-specific risk of liver transplant graft failure. *Liver Transplant*, 2013, 19:987–906. Jackson KR, Motter JD, Haugen CE, Holscher C, Long JJ, Massie AB, Philosophe B, Cameron AM, Garonzik-Wang J, Segev DL. Temporal trends in utilization and outcomes of steatotic donor livers in the United States. *Am J Transplant*, 2020, 20:855–637. Spitzer AL, Lao OB, Dick AAS, Bakthavatsalam R, Halldorson JB, Yeh MM, Upton MP, Reyes JD, Perkins JD. The biopsied donor liver: Incorporating macrosteatosis into high-risk donor assessment. *Liver Transplant*, 2010, 16:874–848. Graham JA, Guarrera J V. “resuscitation” of marginal liver allografts for transplantation with machine perfusion technology. *J Hepatol*, 2014, 619. Muhammad H, Zaffar D, Tehreem A, Ting PS, Simsek C, Turan I, Alqahtani S, Saberi B, Gurakar A. An update on usage of high-risk donors in liver transplantation. *J Clin Med*, 2022, 1110. Kwong AJ, Kim WR, Lake J, Stock PG, Wang CJ, Wetmore JB, Melcher ML, Wey A, Salkowski N, Snyder JJ, Israni AK. Impact of Donor Liver Macrovesicular Steatosis on Deceased Donor Yield and Posttransplant Outcome. *Transplantation*, 2023, 10711. Cesaretti M, Addeo P, Schiavo L, Anty R, Iannelli A. Assessment of Liver Graft Steatosis: Where Do We Stand? *Liver Transplant*, 2019, 25:500–912. Neil DAH, Minervini M, Smith ML, Hubscher SG, Brunt EM, Demetris AJ. Banff consensus recommendations for steatosis assessment in donor livers. *Hepatology*, 2022, 75:1014–2513. Rajamani AS, Rammohan A, Sai VVR, Rela M. Current techniques and future trends in the diagnosis of hepatic steatosis in liver donors: A review. *J Liver Transplant*, 2022, 7:10009114. McLaughlin BL, Wells AC, Virtue S, Vidal-Puig A, Wilkinson TD, Watson CJE, Robertson PA. Electrical and optical spectroscopy for

quantitative screening of hepatic steatosis in donor livers. *Phys Med Biol*, 2010, 5515. Le Naour F, Gadea L, Danulot M, Yousef I, Vibert E, Wavelet M, Kaščáková S, Castaing D, Samuel D, Dumas P, Guettier C. Quantitative assessment of liver steatosis on tissue section using infrared spectroscopy. *Gastroenterology*, 2015, 14816. Golse N, Cosse C, Allard MA, Laurenzi A, Tedeschi M, Guglielmo N, Fernandez-Sevilla E, Robert M, Tréchet B, Pietrasz D, Pittau G, Ciaccio O, Sa Cunha A, Castaing D, Cherqui D, Adam R, Samuel D, Sebah M, Vibert E. Evaluation of a micro-spectrometer for the real-time assessment of liver graft with mild-to-moderate macrosteatosis: A proof of concept study. *J Hepatol*, 2019, 70:423–3017. Evers DJ, Westerkamp AC, Spliethoff JW, Pully V V., Hompes D, Hendriks BHW, Prevoo W, Van Velthuysen MLF, Porte RJ, Ruers TJM. Diffuse reflectance spectroscopy: Toward real-time quantification of steatosis in liver. *Transpl Int*, 2015, 2818. Reistad N, Nilsson JH, Bergenfeldt M, Rissler P, Stureson C. Intraoperative liver steatosis characterization using diffuse reflectance spectroscopy. *HPB*, 2019, 2119. Butler HJ, Ashton L, Bird B, Cinque G, Curtis K, Dorney J, Esmonde-White K, Fullwood NJ, Gardner B, Martin-Hirsch PL, Walsh MJ, McAinsh MR, Stone N, Martin FL. Using Raman spectroscopy to characterize biological materials. *Nat Protoc*, 2016, 11:664–8720. Hewitt KC, Ghassemi Rad J, McGregor HC, Brouwers E, Sapp H, Short MA, Fashir SB, Zeng H, Alwayn IP. Accurate assessment of liver steatosis in animal models using a high throughput Raman fiber optic probe. *Analyst*, 2015, 140:6602–921. Pacia MZ, Czamara K, Zebala M, Kus E, Chlopicki S, Kaczor A. Rapid diagnostics of liver steatosis by Raman spectroscopy via fiber optic probe: a pilot study. *Analyst*, 2018, 143:4723–3122. Szafraniec E, Tott S, Kus E, Augustynska D, Jaształ A, Filipek A, Chlopicki S, Baranska M. Vibrational spectroscopy-based quantification of liver steatosis. *Biochim Biophys Acta - Mol Basis Dis*, 2019, 186523. Majzner K, Kochan K, Kachamakova-Trojanowska N, Maslak E, Chlopicki S, Baranska M. Raman imaging providing insights into chemical composition of lipid droplets of different size and origin: in hepatocytes and endothelium. *Anal Chem*, 2014, 86:6666–7424. Szafraniec E, Kus E, Wislocka A, Kukla B, Sierka E, Untereiner V, Sockalingum GD, Chlopicki S, Baranska M. Raman spectroscopy-based insight into lipid droplets presence and contents in liver sinusoidal endothelial cells and hepatocytes. *J Biophotonics*, 2019, 1225. Minamikawa T, Ichimura-Shimizu M, Takanari H, Morimoto Y, Shiomi R, Tanioka H, Hase E, Yasui T, Tsuneyama K. Molecular imaging analysis of microvesicular and macrovesicular lipid droplets in non-alcoholic fatty liver disease by Raman microscopy. *Sci Rep*, 2020, 1026. Guo H, Tikhomirov AB, Mitchell A, Alwayn IPJ, Zeng H, Hewitt KC. Real-time assessment of liver fat content using a filter-based Raman system operating under ambient light through lock-in amplification. *Biomed Opt Express*, 2022, 13:5231–4527. Nahon JE, Groeneveldt C, Geerling JJ, van Eck M, Hoekstra M. Inhibition of protein arginine methyltransferase 3 activity selectively impairs liver X receptor-driven transcription of hepatic lipogenic genes in vivo. *Br J Pharmacol*, 2018, 17528. de Jong LM, Zhang Z, den Hartog Y, Sijzenaar TJP, Martins Cardoso R, Manson ML, Hankemeier T, Lindenburg PW, Salvatori DCF, Van Eck M, Hoekstra M. PRMT3 inhibitor SGC707 reduces triglyceride levels and induces pruritus in Western-type diet-fed LDL receptor knockout mice. *Sci Rep*, 2022, 1229. Out R, Hoekstra M, Hildebrand RB, Kruit JK, Meurs I, Li Z, Kuipers F, Van Berkel TJC, Van Eck M. Macrophage ABCG1 deletion disrupts lipid homeostasis in alveolar macrophages and moderately influences atherosclerotic lesion development in LDL receptor-deficient mice. *Arterioscler Thromb Vasc Biol*, 2006, 2630. Scientific American MasterTech. Oil Red O Stain Procedure, 2019:1–4. <https://www.statlab.com/pdfs/ifu/storo.pdf>. (accessed July 24, 2023)31. Ramírez-Zacarias JL, Castro-Muñozledo F, Kuri-Harcuch W. Quantitation of adipose conversion and triglycerides by staining intracytoplasmic lipids with oil red O. *Histochemistry*, 1992, 9732. Riva G, Villanova M, Cima L, Ghimenton C, Bronzoni C, Colombari R, Crestani M, Sina S, Brunelli M, D’Errico A, Montin U, Novelli L, Eccher A. Oil Red O Is a Useful Tool to Assess Donor Liver Steatosis on Frozen Sections During Transplantation. *Transplant Proc*, 2018, 5033. Levene AP, Kudo H, Thursz MR, Anstee QM, Goldin RD. Is oil red-O staining and digital image analysis the gold standard for quantifying steatosis in the liver? *Hepatology*, 2010, 5134. Abdelmalek MF. Is oil red-O staining and digital image analysis the gold standard for quantifying steatosis in the liver? Reply. *Hepatology*, 2010, 5135. Choi SS, Diehl AM. Hepatic triglyceride synthesis and nonalcoholic fatty liver disease. *Curr Opin Lipidol*, 2008, 19:295–30036. van Staveren HJ, Moes CJM, van Marie J, Prahł SA, van Gemert MJC. Light scattering in Intralipid-10% in the wavelength range of 400–1100 nm. *Appl Opt*, 1991, 3037. Kuwashiro T, Takahashi H, Hyogo H, Ogawa Y, Imajo K, Yoneda M, Nakahara T, Oeda S, Tanaka K, Amano Y, Ogawa S, Kawaguchi A, Aishima S, Kage M, Chayama K, Nakajima A, Eguchi Y.

Discordant pathological diagnosis of non-alcoholic fatty liver disease: A prospective multicenter study. JGH Open, 2020, 438. El-Badry AM, Breitenstein S, Jochum W, Washington K, Paradis V, Rubbia-Brandt L, Puhon MA, Slankamenac K, Graf R, Clavien PA. Assessment of hepatic steatosis by expert pathologists: the end of a gold standard. Ann Surg, 2009, 250:691–6

Supplementary materials

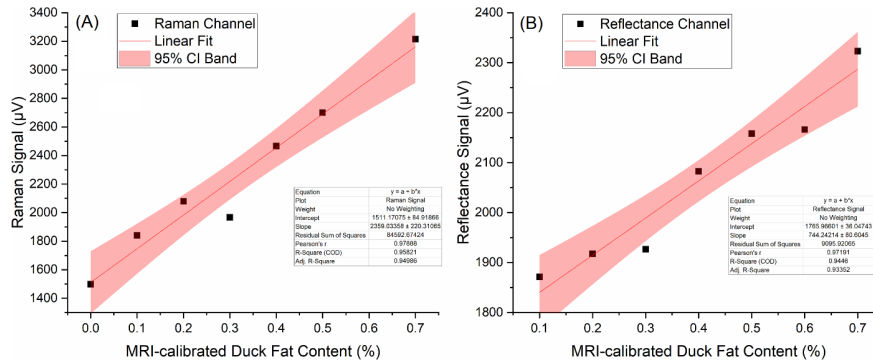


Figure S1. Examples of calibrations using the duck fat phantoms. (A) The Raman channel; (B) the reflectance channel

Table S1. Comparisons among single- and double-variable classification methods. \*p-value < 0.05, indicating the compared AUROCs are statistically significantly different.

	Area Under ROC Curve		p-value (H <sub>0</sub> : Equal AUROC)				
Threshold	Raman (#1)	Reflectance (#2)	Dual (#3)	#1, 2	#1, 3	#2, 3	#1, 2, 3
Macrosteatosis							
10%	0.90 [0.82-0.99]	0.84 [0.91-0.96]	0.94 [0.88-0.99]	0.381	0.204	0.066	<0.001
30%	0.88 [0.80-0.96]	0.84 [0.75-0.94]	0.91 [0.84-0.98]	0.564	0.153	0.085	<b>0.001</b>
60%	0.90 [0.75-1.00]	0.75 [0.54-0.95]	0.89 [0.73-1.00]	0.151	0.532	0.151	0.336
All steatosis							
10%	0.90 [0.80-0.99]	0.78 [0.57-1.00]	0.91 [0.82-1.00]	0.365	0.552	0.277	0.214
30%	0.88 [0.80-0.96]	0.83 [0.71-0.94]	0.91 [0.85-0.98]	0.491	0.260	0.104	<b>0.011</b>
60%	0.91 [0.79-1.00]	0.79 [0.61-0.96]	0.90 [0.78-1.00]	0.170	0.702	0.139	0.196
Stained pixels							
10%	0.89 [0.70-1.00]	0.97 [0.92-1.00]	0.98 [0.94-1.00]	0.388	0.378	0.480	0.670
30%	0.90 [0.83-0.97]	0.79 [0.67-0.91]	0.91 [0.84-0.98]	0.093	0.657	0.025	<b>0.021</b>
60%	0.99 [0.98-1.00]	0.88 [0.75-1.00]	1.00 [1.00-1.00]	0.091	0.413	0.070	0.084